

# Overview on Microstructure- and Defect-Sensitive Fatigue Modeling of Additively Manufactured Materials

BRIAN TORRIES,<sup>1,2</sup> AIDIN IMANDOUST,<sup>1,2</sup> STEFANO BERETTA,<sup>3</sup>  
SHUAI SHAO,<sup>4</sup> and NIMA SHAMSAEI<sup>1,2,5</sup> 

1.—Department of Mechanical Engineering, Auburn University, Auburn, AL 36849, USA. 2.—National Center for Additive Manufacturing Excellence (NCAME), Auburn University, Auburn, AL 36849, USA. 3.—Department of Mechanical Engineering, Politecnico di Milano, Milan, Italy. 4.—Department of Mechanical and Industrial Engineering, Louisiana State University, Baton Rouge, LA 70803, USA. 5.—e-mail: shamsaei@auburn.edu

The possibility of predicting the fatigue behavior of additively manufactured materials by means of microstructure- and defect-sensitive models is discussed in this paper. The effects of surface roughness, process-induced defects, and microstructure on the fatigue life of additively manufactured materials are presented, along with discussions on efforts to incorporate the subsequent effects of these features on fatigue performance using fracture mechanics approach, the multistage fatigue model, and numerical modeling and analysis. Such efforts in fatigue modeling are critical to evaluate the reliability of additive manufactured parts in order to further expand their industrial adoption.

## INTRODUCTION

Additive manufacturing has attracted a great deal of attention in recent years, mainly due to its capability to fabricate complex geometries, which are often unobtainable through traditional subtractive methods.<sup>1–3</sup> Production of functionally graded materials<sup>4–9</sup> and designed internal porosity<sup>4,6,7,10,11</sup> are both viable through additive manufacturing. Besides its production capacity, additive manufacturing is a versatile tool for repairing expensive parts so as to prolong their service life.<sup>6,12,13</sup> However, despite its potential, additive manufacturing has not yet achieved full industrial adoption.

One of the major obstacles to implementation of additive manufacturing is the unique structural features stemming from additive processes, such as porosity, lack of fusion (LOF), surface roughness, and atypical microstructure. Defects such as porosity and LOF are detrimental to mechanical properties, as they introduce uncertainty due to their stochastic nature.<sup>14–16</sup> In fact, the pores, LOF, and surface roughness inherent to additive manufacturing can act as stress raisers, greatly reducing the fatigue strength.<sup>14,17–19</sup> Additively manufactured (AM) parts experience relatively higher cooling rates than conventionally manufactured

parts, yielding unique microstructural features such as microscale segregation and finer grain size.<sup>20</sup> These factors can cause more uncertainty in fatigue strength, increasing the challenge of designing durable and reliable AM parts. Production of defect-free AM parts is hardly possible. Therefore, identifying and incorporating the individual and synergic effects of defects, surface topography, and microstructure on the fatigue strength of AM parts is essential to facilitate its broader industrial use. This may be achieved by calibrating, modifying, or integrating available microstructure- and defect-sensitive fatigue life methodologies.<sup>21,22</sup>

While no single fatigue model may consider all of the above-mentioned structural features, different fatigue models have been successfully applied to account for one or more of these structural features. One method that has been successful in modeling porosity and surface roughness effects is the  $\sqrt{\text{area}}$  model by Murakami et al.,<sup>23–25</sup> which uses the square root of the defect area projected onto the loading plane to calculate the stress intensity factor at defects of irregular size, then calculates the fatigue limit by expressing  $\Delta K_{th}$  as dependent on the hardness of the material. Finite element analysis (FEA) has been applied to determine the effects

of surface roughness on fatigue behavior.<sup>26</sup> In this approach, surface roughness measurements are used to determine stress concentrations and crack propagation thresholds via FEA, which are then used to predict the fatigue life of components. The multistage fatigue (MSF) model was developed by McDowell et al.<sup>27</sup> to address the effects of microstructure on fatigue behavior through use of internal state variables.<sup>28</sup> Such considerations are crucial for evaluating the fatigue performance of AM parts, as slight alterations to process parameters and/or geometry can affect the thermal history and, thereby, the microstructure, defects, and fatigue properties; For instance, different build orientations<sup>29–33</sup> or interlayer time intervals<sup>17,34,35</sup> during fabrication, while keeping the other design and process parameters constant, can change the fatigue behavior of otherwise identical specimens.

The randomness of process-induced defects introduces significant scatter into the fatigue data of AM specimens, introducing an important challenge to the usefulness of empirical fatigue models. While empirical fatigue models allow for fatigue life predictions of parts fabricated with a particular process setting, they may not necessarily be applicable to parts fabricated utilizing different process and design parameters.<sup>17,19</sup> Therefore, the effects of the aforementioned structural features on fatigue behavior need to be truly understood in order to allow for service life predictions of AM products by means of nondestructive defect analysis and appropriate microstructure/defect-sensitive fatigue life assessment.

This overview paper is not a literature review, and is by no means a comprehensive collection of fatigue models. The aim here is rather to critically discuss the potential of a few fatigue models to capture the effects of surface roughness, process-driven defects, and microstructure on the fatigue behavior of AM parts fabricated via multiple additive manufacturing methods.

## PHYSICAL FACTORS AFFECTING FATIGUE LIFE

### Surface Roughness

One of the factors affecting the fatigue life of AM products is the relatively rough surface finish due to the layer-upon-layer build strategy utilized by the additive manufacturing process.<sup>22,36–47</sup> Surface roughness can be divided into two categories: primary roughness, arising from the cooling of the melt pool on the part's edge, and secondary roughness, stemming from partially melted powder particles adhering to the surface.<sup>38</sup> To alleviate surface roughness effects on the fatigue life of AM materials, surface treatments are commonly used to remove peaks and valleys associated with the as-built rough surface. It has been reported that AM specimens in as-built condition possess lower fatigue life than specimens subjected to various surface

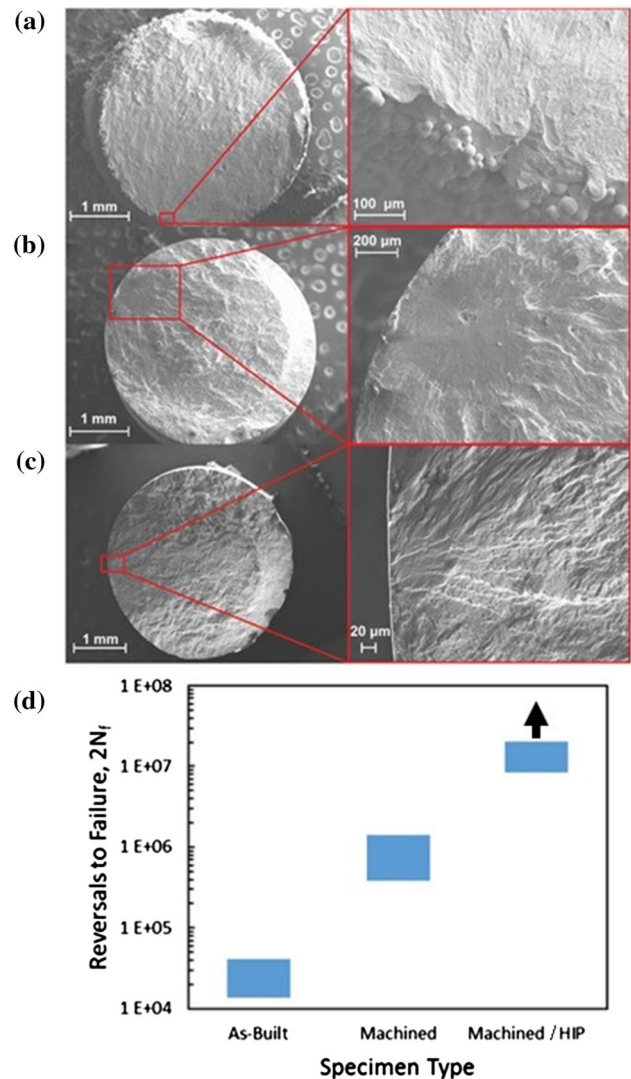


Fig. 1. Comparison of crack initiation sites for (a) as-built, (b) machined, and (c) machined HIP AM Ti-6Al-4V specimens. (d) The fatigue life range for these specimens at strain amplitude of 0.005 mm/mm. Arrow represents runout tests<sup>48</sup>.

treatments.<sup>36–43</sup> Cracks were noted to initiate from surface defects rather than from internal porosity.<sup>36,37,39</sup> An example of this can be seen in Fig. 1a, reported by Torries et al.<sup>48</sup>

Based on existing literature, the most effective surface treatment is milling the surface of AM parts.<sup>38–40</sup> Other studied surface treatment methods include micromachining,<sup>40</sup> blasting,<sup>39,40</sup> electropolishing,<sup>39</sup> and vibratory grinding,<sup>40</sup> all of which improve the fatigue life of parts to varying degrees. However, no direct correlation between specific surface roughness values and fatigue life was found.<sup>40</sup> This could be due to the fact that surface treatments affect material properties or create residual stresses,<sup>40</sup> or that by lessening the effects of surface roughness other factors (such as internal porosity) are allowed greater influence.

While surface roughness can be machined or polished away in some cases, the necessity for surface treatment puts the versatility of the additive manufacturing technique under question. Despite the persistent and uncontrollable nature of the rough surface finish, accurately modeling of its subsequent effects would allow for use of as-built AM components without postfabrication surface treatment. Additionally, some applications, such as bone implants, may benefit from surface roughness, using it to promote better implant integration.<sup>11</sup>

### Process-Induced Internal Defects

Process-inherent defects such as pores and LOF stem from use of suboptimal processing parameters.<sup>16,49</sup> Porosity can be generated via vapor recoil<sup>50</sup> or high-speed flow<sup>51</sup> in the melt pool, or gas pores contained within powder particles used during fabrication.<sup>18,49</sup> As an internal stress raiser, porosity plays a major role in fatigue failure of AM materials by shortening the fatigue crack initiation life.<sup>14,18,22,29,32,45–47,52–56</sup> Multiple studies have reported that cracks tend to initiate from subsurface porosity in machined/polished AM specimens.<sup>18,22,29,32,45,56,57</sup> An example of this is shown in Fig. 1b.<sup>48</sup>

LOF is a process-induced defect caused by insufficient remelting of previously deposited layers,<sup>58–60</sup> insufficient melt pool energy density,<sup>61</sup> or insufficient laser track overlap,<sup>58</sup> leaving thin, often irregularly shaped voids, which can be detrimental to the fatigue strength of AM parts. The orientation of LOF defects, which often corresponds with layer orientation, can introduce anisotropy into the fatigue response of AM products. LOF defects typically form at boundaries between layers and individual scan tracks,<sup>58</sup> which ties their orientation to the build, or layer, orientation. As the LOF orientation changes with respect to the loading, so does the projected area on the loading plane; increased area leads to lower fatigue resistance. The magnitude of this change is correlated to the notch sensitivity of the material; greater notch sensitivity means the magnitude of this change will be greater. Layer orientation had little<sup>38</sup> to no effect<sup>36,57</sup> on the fatigue behavior of AM Ti-6Al-4V fabricated via powder bed fusion (PBF). No LOF were reported by Konečná et al.,<sup>38</sup> and very little LOF was reported by Wycisk et al.<sup>36</sup> and Torries et al.<sup>57</sup>; therefore, it appears that lack of anisotropy is at least partially related to the absence of LOF. However, studies of other materials revealed anisotropy in the fatigue response as a result of changes in layer orientation. Brandl et al.<sup>30</sup> compared the fatigue life of AlSi10Mg specimens built via PBF in three orientations: horizontal, diagonal (45° angle), and vertical. Vertical specimens displayed the lowest fatigue life, with diagonal specimens exhibiting slight improvement. Horizontal specimens possessed the longest fatigue life.<sup>30</sup> Shrestha et al.<sup>31</sup>

(for AM stainless steel 316L), Yadollahi et al. (for AM 17-4 PH stainless steel),<sup>32</sup> and Meneghetti (for AM maraging steel MS1)<sup>33</sup> also reported notable build orientation effects on the fatigue life of PBF-fabricated specimens. Note that all of these studies reported LOF or unmelted regions present in the material.

Hot isostatic pressing (HIP) has been proven to enhance fatigue resistance by shrinking or closing internal porosity contained within AM parts through simultaneous application of high temperature and pressure. With the effects of porosity reduced via the HIP process, cracks tend to initiate from the specimen surface (Fig. 1c).<sup>48</sup> While it has been shown that HIP can greatly improve fatigue life of both machined and as-built specimens,<sup>44,45,62,63</sup> this is not always the case. HIP can be less effective due to nonoptimal HIP parameters<sup>64</sup> or surface notches resulting from subsurface pores exposed due to machining.<sup>65</sup> Also, as-built Ti-6Al-4V specimens subject to HIP may show only marginal improvements to fatigue life due to cracks initiating from the rough surface rather than internal porosity.<sup>37,40,43,62,66,67</sup> HIP can reduce the scatter in fatigue life due to pore closure. Porosity leads to uncertainty in the fatigue life of AM parts,<sup>18,32,68</sup> especially in the long-life regime<sup>18,35,36</sup> (see Fig. 1d).<sup>48</sup> While the machined specimens did exhibit improved fatigue life as compared with the as-built specimens, there was more scatter in the fatigue life of machined specimens as compared with the as-built and machined HIP specimens.

Despite porosity's detrimental effects on fatigue life, one can take advantage of a porous structure for some specific applications; For instance, introducing internal porosity into a biomedical implant can lower the Young's modulus of the implant to be closer to<sup>4,11</sup> or even equal<sup>10</sup> to that of bone, allowing for improved integration.<sup>4,10,11</sup> Therefore, while it is critical to work towards controlling the porosity volume fraction in AM parts, it is equally important to be able to model its effects on the mechanical properties.

### Microstructure

Although process parameters can be optimized to reduce the formation of defects, AM materials experience a very high cooling rate during their manufacture regardless of the selected process parameters. In addition, any variation in process parameters and/or part geometry can affect the experienced thermal history, resulting in AM parts possessing different microstructure and mechanical/fatigue behavior than their wrought counterparts. Therefore, the subsequent effect of microstructure on fatigue life needs to be truly characterized before fatigue data generated from specimens can be used for designing AM parts.<sup>22</sup> Any variation in cooling rate during fabrication may result in different volume fractions, morphologies,



and characteristics of the constituent phases; For instance, a higher cooling rate during additive manufacturing of Ti-6Al-4V yields a nearly completely martensitic structure for both direct laser deposition and PBF,<sup>16,69–72</sup> while increasing the deposited layer thickness from 30  $\mu\text{m}$  to 60  $\mu\text{m}$  may provide adequate heat accumulation for decomposition of  $\alpha'$  to  $\alpha + \beta$  in PBF.<sup>73,74</sup> Compared with  $\alpha + \beta$  microstructure, fine needle-like martensitic grains would improve fatigue crack initiation life by virtue of the reduced effective slip length being limited to the  $\alpha'$  lath thickness.<sup>73</sup> Relatively coarser  $\alpha + \beta$  lamellar or basket-weave microstructure yields reduced ductility and strength.<sup>73</sup>

The competition between the solidification rate (speed of the solidification front) and the thermal gradient (nucleation rate) can significantly alter the solidified microstructure.<sup>75,76</sup> In areas with a higher cooling rate, the faster nucleation rate produces equiaxed grain structures. This is more common closer to the substrate, where the cooling rate is high due to the higher rate of conductive heat transfer through the substrate.<sup>77</sup> On the other hand, columnar grains often form farther from the substrate, partly due to the lower cooling rate and directional solidification.<sup>70</sup> Columnar grains have the propensity to copy their parent grains texture and, especially in Ti alloys, produce sharp texture, which introduces anisotropy into the monotonic deformation behavior of the part.<sup>58,78</sup> However, the presence of defects in AM materials, such as LOF, may override the effects of microstructural variables.

Postprocess heat treatment, which is widely used to improve the fatigue properties of AM materials, is another major factor affecting microstructural evolution. Large residual stresses can be developed during additive manufacturing.<sup>44–47,79,80</sup> While heat treatment can remove these stresses, it can also alter the fatigue properties of the material by altering the distribution and individual properties of the phases. However, a generic heat treatment of specimens might be deleterious to the fatigue resistance of AM products. Sterling et al.<sup>18</sup> found that Ti-6Al-4V specimens, annealed at 704°C for 1 h followed by air cooling, exhibited lower high-cycle fatigue life than specimens not subjected to any heat treatment. This decrease in fatigue life was attributed to relief of beneficial compressive residual stresses present in the specimens. In the same study, an alternative heat treatment consisting of a 2-h soak at 1050°C followed by furnace cooling resulted in lamellar microstructure, improving material strength and fatigue properties in the long-life regime. Loss of ductility led to slightly lower fatigue life in the low-cycle regime.<sup>18</sup> Additionally, AM products with different thermal history may require entirely different heat treatment cycles to improve their fatigue performance.

## DEFECT- AND MICROSTRUCTURE-SENSITIVE FATIGUE MODELS

As a major fatigue design factor, modeling the fatigue behavior of engineering alloys has long been an ongoing research topic. As such, the fatigue behavior of an AM alloy needs to be well documented before it can be considered a viable option in engineering materials selection and processing. However, the fatigue behavior of an AM metal can vary significantly with any change in process and design parameters, as they affect microstructural and defect properties. Some traditional fatigue models are unable to capture such effects and, therefore, cannot accurately capture the fatigue behavior of AM materials. Other models, such as the fracture mechanics approach, the MSF model, and numerical modeling, may take some of these structural features into consideration and, thus, be more applicable for characterizing the fatigue behavior of AM materials.

### Fracture Mechanics Approach

To more accurately predict the fatigue life and its range for AM materials, contained defect and surface roughness effects must be considered. One method that considers process defect effects on fatigue life is the  $\sqrt{\text{area}}$  model by Murakami,<sup>23–25,81,82</sup> according to which the fatigue limit of materials with heterogeneous defects, such as pores and inclusions, is a factor of the hardness (as a representative for material strength) and discontinuities.<sup>81</sup> The  $\sqrt{\text{area}}$  model by Murakami<sup>23</sup> determines the fatigue strength of a part with small defects such as pores and inclusions by determining the threshold stress for the small cracks that naturally develop at the tip of the defects. By treating the defects as irregular cracks, a representative dimension is taken as the square root of the area of the defect projected in the direction of maximum tensile stress. The accompanying stress intensity factor is expressed as

$$K_{\max} = 0.65\sigma\sqrt{\pi\sqrt{\text{area}}} \quad \text{for a surface crack,} \quad (1)$$

$$K_{\max} = 0.5\sigma\sqrt{\pi\sqrt{\text{area}}} \quad \text{for an internal crack,} \quad (2)$$

where  $K_{\max}$  is the maximum stress intensity factor,  $\sigma$  is stress, and  $\sqrt{\text{area}}$  is the aforementioned representative dimension of the crack.<sup>81</sup> Murakami and Endo<sup>24</sup> expressed the  $\Delta K_{\text{th}}$  of a material as

$$\Delta K_{\text{th}} \propto (\text{HV} + C_1) \times (\sqrt{\text{area}})^{1/3}, \quad (3)$$

where HV is the material hardness and  $C_1$  is a material constant. Combining Eqs. 1 and 2 with Eq. 3 and expressing the fatigue limit as the stress at which  $\Delta K = \Delta K_{\text{th}}$ , the fatigue limit,  $\sigma_{\text{FL}}$ , can be expressed as<sup>81</sup>

$$\sigma_{FL} = 1.43 \frac{(HV + 120)}{(\sqrt{\text{area}})^{1/6}} \quad \text{for surface cracks,} \quad (4)$$

$$\sigma_{FL} = 1.56 \frac{(HV + 120)}{(\sqrt{\text{area}})^{1/6}} \quad \text{for internal cracks.} \quad (5)$$

The  $\sqrt{\text{area}}$  model allows for easy expression of the relationship between the fatigue limit and defect size via the Kitagawa–Takahashi diagram.<sup>83</sup> Other models<sup>24,84,85</sup> can also be used to express this relationship, which has a general form of the type<sup>80</sup>

$$\sigma_{FL} \propto \frac{1}{(\sqrt{\text{area}})^{1/n'}}, \quad (6)$$

where  $n' = 2$  for long cracks [the region of applicability of linear elastic fracture mechanics (LEFM)] and  $n'$  approaches infinity for very small cracks. In the latter case, the fatigue limit tends towards the fatigue limit of smooth specimens (i.e., typically, 0.5 ultimate tensile strength for steels), with competition between defects and microstructural features.<sup>86,87</sup>

Beretta and Romano<sup>80</sup> used the  $\sqrt{\text{area}}$  model by Murakami in conjunction with the Kitagawa–Takahashi diagram to accurately predict the crack growth threshold of AM materials. This can be seen in Fig. 2 (elaborated from the data in Ref. 80), where the  $\sqrt{\text{area}}$  approach was used to determine the fatigue strength and crack propagation factors of AM AlSi10Mg and Ti-6Al-4V. Note that as the equivalent defect size increases, the fatigue limit decreases. Conversely, the crack growth threshold increases and approaches the long crack growth threshold as the equivalent defect size increases. In particular, Beretta and Romano<sup>80</sup> found that the  $\Delta K_{th} - \sqrt{\text{area}}$  and  $\sigma_{FL} - \sqrt{\text{area}}$  relationships were similar for AM and wrought AlSi10Mg and Ti-6Al-4V at  $R = 0.1$  and  $R = -1$ . Romano et al.<sup>29</sup> conducted a study on the porosity of AM AlSi10Mg specimens, seeking to determine the fatigue critical pore size detected via x-ray computed tomography (CT). Using “statistics of extremes,” the distribution of the maximum defect size was estimated and found to be consistent with the defects at the origin of the fatigue failures.<sup>19</sup> The  $\sqrt{\text{area}}$  approach was then applied to treat the pores as small cracks, allowing for the fatigue strength to be found via adoption of the El Haddad model<sup>88</sup> to describe the Kitagawa–Takahashi diagram.<sup>19,29</sup>

In addition to accounting for internal porosity, the  $\sqrt{\text{area}}$  model by Murakami has shown the capacity to consider surface roughness effects.<sup>89,90</sup> Surface roughness measurements may be used to create an equivalent internal flaw size, which is then used to determine the fatigue strength via the  $\sqrt{\text{area}}$  model.<sup>89</sup> A study by Greitemeier et al.<sup>90</sup> used this equivalent flaw size and the Forman–Metttu equation<sup>91</sup> to predict the fatigue life of as-built AM

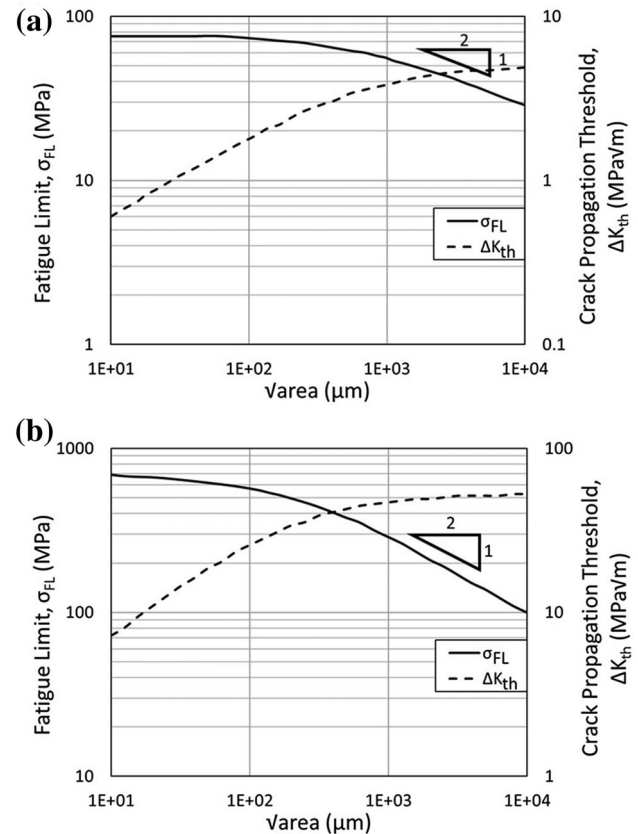


Fig. 2. Fatigue strength and crack propagation thresholds as a function of representative defect dimension for (a) AlSi10Mg and (b) Ti-6Al-4V fatigue specimens fabricated via additive manufacturing, tested at  $R = -1$ . Adapted from Ref. 80.

specimens. An average fit was found using an equivalent internal flaw size derived from the average surface roughness measurements, with upper and lower bounds corresponding to surface roughness deviations. This fit matched the data well, with all data points falling within these bounds.<sup>90</sup>

While these studies highlight the applicability of the  $\sqrt{\text{area}}$  model by Murakami to additive manufacturing, this approach in its current state may not account for some influencing factors. The  $\sqrt{\text{area}}$  model predicts the fatigue limit, not the fatigue life at specific loadings. The fatigue life can be found by application of crack propagation models, such as the theory of critical distance (TCD)<sup>92–96</sup> or the Forman–Metttu equation or NASGRO, provided that the crack is assumed to be semicircular with the same  $\sqrt{\text{area}}$  as the largest observed defect (see Ref. 19). Scatter bands can also be generated using different defect sizes (2.5%, 50%, and 97.5% percentiles of the defect size), as seen in Fig. 3.<sup>19,80</sup> The specimens shown in this figure (P1, P2, and P3) were fabricated with different process parameters. Further discussion of the manufacturing processes and differences are available in Ref. 19. The average defect size observed in specimens P1, P2, and P3

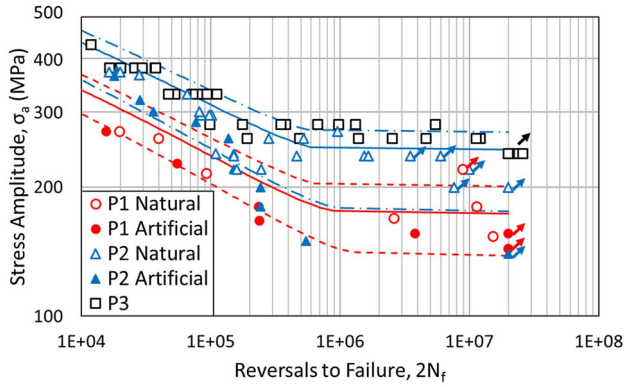


Fig. 3. Fatigue life estimates obtained by LEFM analysis of the largest LOFs as cracks in two different AM processes for AlSi10Mg. Average defect size for specimens P1, P2, and P3 was 500  $\mu\text{m}$ , 250  $\mu\text{m}$ , and 90  $\mu\text{m}$ , respectively. Arrows represent runout tests. Adapted from Refs. 19 and 80.

and used to generate the fits was 500  $\mu\text{m}$ , 250  $\mu\text{m}$ , and 90  $\mu\text{m}$ , respectively. For defects such as these, Murakami's model does not take into account the microstructure. These considerations become important when defects have dimensions comparable to the grain size.<sup>86,87</sup> On the other hand, the power law of  $\Delta K_{\text{th}}$  regarding defect size with a slope of 1/3 is only valid over a limited defect size range (up to 400  $\mu\text{m}$  for AlSi10Mg and 300  $\mu\text{m}$  for Ti6Al4V). For larger defects, it is necessary to adopt other formulations, as explained in Ref. 19.

### Multistage Fatigue Model

The MSF model proposed by McDowell et al.<sup>27</sup> is a microstructure-sensitive fatigue model that uses a reference grain size and orientation, pore size and nearest neighbor distance, total porosity, and particle size to determine the fatigue life of a material with consideration of the different stages of fatigue damage evolution (crack incubation, microstructurally small crack growth, and long crack growth). The MSF model determines the total life as

$$N_{\text{Total}} = N_{\text{INC}} + N_{\text{MSC}} + N_{\text{LC}}, \quad (7)$$

where  $N_{\text{Total}}$  is the total cycles to failure,  $N_{\text{INC}}$  is the crack incubation cycles,  $N_{\text{MSC}}$  is the number of cycles spent in the microstructurally small crack growth stage, and  $N_{\text{LC}}$  is the number of cycles spent in the long crack growth stage until failure. The nucleation and propagation of these cracks are modeled using a two stage Coffin–Manson relationship:

$$C_{\text{INC}} N_{\text{INC}}^{\alpha} = \beta, \quad (8)$$

$$\left(\frac{da}{dN}\right)_{\text{MSC}} = \chi(\Delta\text{CTD} - \Delta\text{CTD}_{\text{th}}), \alpha_i = 0.625D, \quad (9)$$

where  $C_{\text{INC}}$  and  $\alpha$  are the linear and exponential material constants, respectively,  $\beta$  is the nonlocal damage parameter based upon the ratio of the

plastic zone size around a defect and the diameter of the corresponding defect,  $\left(\frac{da}{dN}\right)_{\text{MSC}}$  is the microstructurally small crack growth rate,  $\chi$  is a material constant,  $\Delta\text{CTD}$  and  $\Delta\text{CTD}_{\text{th}}$  are the crack tip displacement range and threshold, respectively,  $\alpha_i$  is the initial crack length, and  $D$  is the diameter of the pore serving as the initiation site. See Refs. 15, 27, 97 and 98 for more in-depth discussion on this model. While the MSF model was designed for A356-T6 aluminum alloy,<sup>27,97</sup> it has also been applied to A380-F aluminum alloy,<sup>97</sup> plastics (acrylonitrile butadiene styrene),<sup>98,99</sup> and even AM materials by Xue et al.<sup>15</sup> and Torries et al.<sup>14,17</sup>

Because the MSF model utilizes defect size information and compares the grain size and orientation of the material in question to a reference size and distribution, it can account for microstructural changes caused by different thermal histories and predict a mean fatigue life with upper and lower bounds corresponding to the smallest and largest observed internal defects, respectively.<sup>14</sup> Therefore, the MSF model not only predicts the average fatigue life but can also account for data scatter due to fluctuations in defect/microstructural features. Though versatile, the MSF model, in its original form, does not take into consideration the shape of process defects or their orientation. However, a new iteration of the MSF model may be capable of taking the orientation into account.<sup>100</sup> Additionally, while fatigue life predictions made by this model are fairly accurate, the large amount of data used for calibration limits its widespread application.

### Numerical Methods

Fatigue cracks are predominantly driven by localized plasticity and initiate from the specimen surface for wrought materials. This initiation is governed by the intrusion/extrusion mechanisms arising from the formation and operation of sub-grain dislocation structure, such as vein structures and persistent slip bands (PSB).<sup>101–107</sup> For AM materials, surface roughness results in localized stress raisers and can lead to early onset of plastic deformation. Due to the vanishingly small volume fraction of such plastic zones, substantial surface roughness-induced fatigue damage can occur even though the overall cyclic stress–strain response appears to be elastic. Therefore, compared with wrought materials, as-built AM materials typically have significantly lower fatigue life due to roughness-induced accelerated fatigue crack nucleation.

Effective quantification of stress concentrations near as-built or poorly machined surfaces of AM parts may be achieved through FEA. Using an experimentally obtained roughness profile (e.g., via x-ray CT, Fig. 4a), the elastic stress distributions for a sample surface can be readily analyzed by FEA (Fig. 4b).<sup>26,108</sup> This information can then be used to



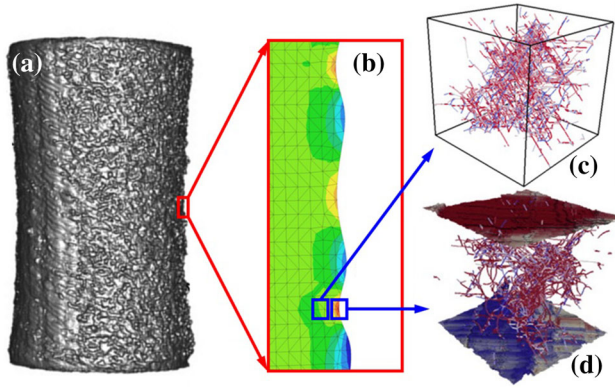


Fig. 4. A hierarchical multiscale modeling scheme combining (a) surface profilometry, (b) FEA-based methods, (c) bulk DD, and (d) surface DD. Adapted from Refs. 22, 26, 117 and 119.

determine the crack propagation threshold in order to evaluate the actual fatigue performance of the component.<sup>26</sup> To this end, several empirical and semiempirical fatigue stress concentration factors,  $K_f$ , for surface roughness have been defined in attempts to predict the fatigue strength of parts with rough surfaces.<sup>95,96</sup> Neuber<sup>92,109</sup> and Peterson<sup>93,110,111</sup> related the notch sensitivity,  $q$ , to the notch root radius by using a material coefficient, which effectively predicted the high-cycle fatigue of notched specimens. However, considering the random surface topography of AM products, the notch root radius is extremely challenging to define.<sup>112</sup> On the other hand, Siebel and Stieler<sup>113</sup> defined  $K_f$  based on the relative stress gradient initiating from surface roughness or stress raisers:

$$K_f = \frac{K_t}{1 + \sqrt{c}\chi}, \quad (10)$$

where  $K_t$  is the stress concentration factor,  $\chi$  is the relative stress gradient, and  $c$  is a constant.  $\chi$  is defined for loading along the  $z$  direction in cylindrical coordinates ( $r, \theta, z$ ) as follows:

$$\chi = \frac{1}{\sigma_{\text{notch}}} \left( \frac{\partial \sigma_z}{\partial r} \right)_{\text{notch}}. \quad (11)$$

Note that the abovementioned quantities are calculated at the notch root, as denoted by the “notch” subscript. The stress gradient can then be computed using FEA for the strain–displacement relations. It was shown that  $K_f$  yielded satisfactory results for a narrow range of fatigue life, while it could not be applied to the entire life regime.

In another study by Suraratchai et al.,<sup>26</sup> the fatigue life of 7010-T7451 aluminum alloy specimens with machining grooves with different orientations was predicted. To characterize the surface roughness, a filtered profile of the specimen surface roughness was determined using local peak and valley height measurements. After calculating the stress concentration factors via FEA,

the crack propagation life,  $N_p$ , for through-thickness and through-width crack propagation was estimated as

$$\frac{da}{dN_p} = C(\Delta K_{90^\circ})^m, \quad (12)$$

$$\frac{dc}{dN_p} = C(K_t \Delta K_{0^\circ})^m, \quad (13)$$

where  $a$  is half the short-axis length of the crack,  $c$  is half the long-axis length of the crack,  $N_p$  is the number of cycles,  $\Delta K$  is the stress intensity factor range,  $K_t$  is the stress concentration factor, and  $C$  and  $m$  are Paris law material constants. The angle subscript denotes the angle at which  $K$  is determined with respect to the long axis of the crack. Equations 12 and 13 are used in an iterative calculation, where the  $a$  and  $c$  values for each cycle are used to calculate a new  $\Delta K_\theta$  calculated from the previous  $a$  and  $c$  values. Calculation stops and  $N_p$  is found when  $a$  is equal to the thickness of the specimen,  $c$  is equal to the width of the specimen, or  $\Delta K_\theta$  is equal to the fracture toughness. Once  $N_p$  has been determined, the crack initiation life is found using

$$N_i = \beta(K_t \sigma_a)^\alpha, \quad (14)$$

where  $N_i$  is the crack initiation life,  $\sigma_a$  is the stress amplitude, and  $\beta$  and  $\alpha$  are material constants that can be found via a Basquin power-law fit. The total predicted fatigue life is found by adding the crack initiation and propagation lives. Fatigue life predictions using this method were satisfactory for all specimen types investigated by Suraratchai et al.<sup>26</sup>

Due to the successes of this model at average surface roughness ( $R_a$ ) values ranging from  $R_a = 0.25 \mu\text{m}$  to  $R_a = 11.1 \mu\text{m}$ ,<sup>26</sup> it is possible that this method could be applied to as-built AM parts, which can have  $R_a$  values ranging from  $10 \mu\text{m}$  to  $13 \mu\text{m}$ <sup>37</sup> for laser-based powder bed fusion. To use this method in its current form, the user assumes that the subsurface defects/pores in the AM parts, particularly those close to the surface, have no effects on the fatigue life and/or stress concentrations from the rough surface. Additionally, this method is not inherently sensitive to the changes in microstructure, although such changes are somewhat reflected in the utilized material constants [i.e.,  $C$ ,  $m$ ,  $\alpha$ , and  $b$  in Eqs. 9–11]. Because both porosity and microstructure have been shown to greatly affect the fatigue properties of AM materials, their inclusion in FEA analysis is necessary to allow for more realistic fatigue life predictions of metals fabricated via additive manufacturing.

While the aforementioned FEA analysis assumes that the mechanical response near the surface of a material is linearly elastic, it is in actuality plastic. This plastic behavior, which dictates the cyclic stress–strain response and the initiation of cracks, is dependent on factors such as local

microstructural features, chemical composition, inclusions, and porosity, all of which can differ between AM materials and their wrought counterparts.<sup>16,22,114–116</sup> Therefore, application of FEA to model the fatigue behavior of AM materials requires incorporation of a priori knowledge regarding dislocation evolution from lower length scale models. One method to account for dislocation dynamics is application of discrete dislocation dynamics (DD) models.

DD simulations have been performed to investigate fatigue damage of wrought materials in terms of the initial cyclic hardening behavior, crack initiation mechanisms, and fatigue crack propagation behavior. Single-crystalline DD models have simulated the evolution of dislocation structures as well as the cyclic hardening behavior during the very early stage of fatigue damage<sup>117–119</sup> (Fig. 4c). This approach provides satisfactory results, but is limited to the initial stage of cyclic loading (the first 5–10 cycles) for realistic initial dislocation density considerations. Using a single-crystalline DD model that utilizes a phenomenological treatment of free surface (without the treatment of image force),<sup>120–124</sup> the cyclic deformation irreversibility due to escape of dislocations through the free surface and initiation of fatigue cracks via intrusion/extrusion mechanisms can be determined (Fig. 4d). Attempted predictions of the critical number of cycles for fatigue crack initiation have been made based on the initial 20–40 cycles of the loading sequence.<sup>125</sup> Additionally, by implementing an artificial crack opening scheme, the fatigue crack propagation behavior may also be simulated.<sup>125</sup>

However, a drawback to direct application of DD to fatigue is the limitation on the total number of simulated cycles. The cost of DD calculations increases significantly with increasing dislocation density, or the number of integration points on dislocation lines due to the dislocation multiplication mechanisms under cyclic loading. The time scale of DD is therefore severely limited.<sup>126–128</sup> Therefore, incorporation of lower length scale information on the evolution of the dislocation structure obtained by DD into FEA-based models<sup>129,130</sup> through a hierarchical multiscale modeling scheme seems necessary (Fig. 4).

## SUMMARY

While additive manufacturing is a versatile process that opens many new design paths, one of the obstacles to its widespread industrial implementation is the uncertainty often observed in fatigue behavior of AM parts as a result of variations in their surface roughness, process defects, and microstructure. Knowledge of fatigue behavior and its dependence on process variables is required for certification and qualification of AM products. Therefore, fatigue modeling methodologies that

are sensitive to the effects of surface roughness, process defects, and microstructure features can be very useful.

While there have been successful attempts to model these effects on the fatigue life of AM parts, an overarching and efficient fatigue model that comprehensively addresses all the abovementioned challenges has not yet been established. To design more reliable and durable AM products, it is essential to identify, develop, and/or update a model that takes into consideration their structural features. This may be accomplished by building on the successes of the methods discussed in this review, as well as pursuing new avenues.

## ACKNOWLEDGEMENTS

This material is based upon work partially supported by the National Science Foundation (NSF) under Grant No. 1657195 and the National Aeronautics and Space Administration (NASA) Award No. NNX17AJ93A and 80MSFC17M0023.

## REFERENCES

1. D.S. Thomas and S.W. Gilbert, NIST SP 1176 National Institute of Standards and Technology (2014).
2. D.S. Thomas, *Int. J. Adv. Manuf.* 85, 1857 (2016).
3. K.S. Chan, M. Koike, R.L. Mason, and T. Okabe, *Metall. Mater. Trans. A* 44, 1010 (2013).
4. B. Vamsi Krishna, W. Xue, S. Bose, and A. Bandyopadhyay, *JOM* 60, 45 (2008).
5. B. Vamsi Krishna, W. Xue, S. Bose, and A. Bandyopadhyay, *Acta Biomater.* 4, 697 (2008).
6. N. Guo and M.C. Leu, *Front. Mech. Eng.* 8, 215 (2013).
7. A. Bandyopadhyay, B. Vamsi Krishna, W. Xue, and S. Bose, *J. Mater. Sci. Mater. Med.* 20, S29 (2009).
8. Y. Huang, M.C. Leu, J. Mazumder, and A. Donmez, *J. Manuf. Sci. Eng.* 137, 1 (2015).
9. W. Gao, Y. Zhang, D. Ramanujan, K. Ramani, Y. Chen, C.B. Williams, C.C.L. Wang, Y.C. Shin, S. Zhang, and P.D. Zavattieri, *Comput.-Aided Des.* 69, 65 (2015).
10. M. Niinomi, *J. Mech. Behav. Biomed. Mater.* 1, 30 (2008).
11. I.-H. Oh, N. Nomura, N. Masahashi, and S. Hanada, *Scr. Mater.* 49, 1197 (2003).
12. R.P. Mudge and N.R. Wald, *Weld. J.* 86, 44 (2007).
13. M. Hedges and N. Calder, ADA524690, Neotech Services MTP Nuremberg (2006).
14. B. Torries, A.J. Sterling, N. Shamsaei, S.M. Thompson, and S.R. Daniewicz, *Rapid Prototyp. J.* 22, 817 (2016).
15. Y. Xue, A. Pascu, M.F. Horstemeyer, L. Wang, and P.T. Wang, *Acta Mater.* 58, 4029 (2010).
16. N. Shamsaei, A. Yadollahi, L. Bian, and S.M. Thompson, *Addit. Manuf.* 8, 12 (2015).
17. B. Torries and N. Shamsaei, *JOM* 69, 2698 (2017).
18. A.J. Sterling, B. Torries, N. Shamsaei, S.M. Thompson, and D.W. Seely, *Mater. Sci. Eng. A* 655, 100 (2016).
19. S. Romano, A. Brückner-Foit, A. Brandão, J. Gumpinger, T. Ghidini, and S. Beretta, *Eng. Fract. Mech.* 187, 165 (2018).
20. S.M. Thompson, L. Bian, N. Shamsaei, and A. Yadollahi, *Addit. Manuf.* 8, 36 (2015).
21. A.B. Spierings, T.L. Starr, and K. Wegener, *Rapid Prototyp. J.* 19, 88 (2013).
22. A. Yadollahi and N. Shamsaei, *Int. J. Fatigue* 98, 14 (2017).
23. Y. Murakami and M. Endo, *Eng. Fract. Mech.* 17, 1 (1983).
24. Y. Murakami and M. Endo, *J. Soc. Mater. Sci.* 35, 911 (1986).
25. Y. Murakami and M. Endo, *Int. J. Fatigue* 16, 163 (1994).
26. M. Suraratchai, J. Limido, C. Mabru, and R. Chieragatti, *Int. J. Fatigue* 30, 2119 (2008).



27. D.L. McDowell, K. Gall, M.F. Horstemeyer, and J. Fan, *Eng. Fract. Mech.* 70, 49 (2003).
28. Y. Xue, D.L. McDowell, M.F. Horstemeyer, M.H. Dale, and J.B. Jordan, *Eng. Fract. Mech.* 74, 2810 (2007).
29. S. Romano, A. Brandão, J. Gumpinger, M. Gschweidl, and S. Beretta, *Mater. Des.* 131, 32 (2017).
30. E. Brandl, U. Heckenberger, V. Holzinger, and D. Buchbinder, *Mater. Des.* 34, 159 (2012).
31. R. Shrestha, J. Simsiriwong, N. Shamsaei, S. M. Thompson, and L. Bian, *Solid Freeform Fabrication Symposium Proceedings* (2016), p. 605.
32. A. Yadollahi, N. Shamsaei, S.M. Thompson, A. Elwany, and L. Bian, *Int. J. Fatigue* 94, 218 (2017).
33. G. Meneghetti, D. Rigon, D. Cozzi, W. Waldhauser, and M. Dabalá, *Procedia Struct. Integr.* 7, 149 (2017).
34. A. Yadollahi, N. Shamsaei, S.M. Thompson, and D.W. Seely, *Mater. Sci. Eng. A* 644, 171 (2015).
35. B. Torries, S. Shao, N. Shamsaei, and S.M. Thompson, *Solid Freeform Fabrication Symposium Proceedings* (2016), p. 1272.
36. E. Wycisk, A. Solbach, S. Siddique, D. Herzog, F. Walther, and C. Emmelmann, *Phys. Procedia* 56, 371 (2014).
37. H. Masuo, Y. Tanaka, S. Morokoshi, H. Yagura, T. Uchida, Y. Tamamoto, and Y. Murakami, *Procedia Struct. Integr.* 7, 19 (2017).
38. R. Konečná, G. Nicoletto, S. Fintová, and M. Frkáň, *Procedia Struct. Integr.* 7, 92 (2017).
39. S. Bagehorn, T. Merens, D. Greitemeier, L. Carton, and A. Schoberth, *Struct. Mater.* 99, 1 (2015).
40. S. Bagehorn, J. Wehr, and H.J. Maier, *Int. J. Fatigue* 102, 135 (2017).
41. A. Fatemi, R. Molaei, S. Sharifimehr, N. Phan, and N. Shamsaei, *Int. J. Fatigue* 100, 347 (2017).
42. A. Fatemi, R. Molaei, S. Sharifimehr, N. Shamsaei, and N. Phan, *Int. J. Fatigue* 99, 187 (2017).
43. M. Kahlin, H. Ansell, and J.J. Moverare, *Int. J. Fatigue* 101, 51 (2017).
44. P. Li, D.H. Warner, A. Fatemi, and N. Phan, *Int. J. Fatigue* 85, 130 (2016).
45. N. Shamsaei and J. Simsiriwong, *Procedia Struct. Integr.* 7, 3 (2017).
46. P. Edwards, A. O'Conner, and M. Ramulu, *J. Manuf. Sci. Eng.* 135, 061016-1 (2013).
47. P. Edwards and M. Ramulu, *Mater. Sci. Eng. A* 598, 327 (2014).
48. B. Torries and N. Shamsaei, Auburn University, Auburn, Unpublished Research (2018).
49. H. Gong, K. Rafi, H. Gu, T. Starr, and B. Strucker, *Addit. Manuf.* 1–4, 87 (2014).
50. L. Han, F.W. Liou, and S. Musti, *J. Heat Transf.* 127, 1005 (2005).
51. S.A. Khairallah, A.T. Anderson, A. Rubenchik, and W.E. King, *Acta Mater.* 108, 36 (2016).
52. S. Leuders, M. Thöne, A. Riemer, T. Niendorf, T. Tröster, H.A. Richard, and H.J. Maier, *Int. J. Fatigue* 48, 300 (2013).
53. H. Gong, K. Rafi, H. Gu, G.D. Janaki Ram, T. Starr, and B. Strucker, *Mater. Des.* 86, 545 (2015).
54. X. Zhao, S. Li, M. Zhang, Y. Liu, T.B. Sercombe, S. Wang, Y. Hao, R. Yang, and L.E. Murr, *Mater. Des.* 95, 21 (2016).
55. A.J. Sterling, B. Torries, N. Shamsaei, S.M. Thompson, and S.R. Daniewicz, *Solid Freeform Fabrication Symposium Proceedings* (2015), p. 636.
56. A.S. Johnson, S. Shao, N. Shamsaei, S.M. Thompson, and L. Bian, *JOM* 69, 597 (2017).
57. B. Torries, N. Shamsaei, and S.M. Thompson, *Solid Freeform Fabrication Symposium Proceedings* (2017), p. 115.
58. B.E. Carroll, T.A. Palmer, and A.M. Beese, *Acta Mater.* 87, 309 (2015).
59. T. Vilaro, C. Colin, and J.D. Bartout, *Metall. Mater. Trans. A* 42A, 3190 (2011).
60. C. Qiu, G.A. Ravi, C. Dance, A. Ranson, S. Dilworth, and M.M. Attallah, *J. Alloys Compd.* 629, 351 (2015).
61. S.K. Everton, M. Hirsch, P. Stravroulakis, R.K. Leach, and A.T. Clare, *Mater. Des.* 95, 431 (2016).
62. K.D. Rekedal, ADA617714, Department of the Air Force AIR University, Ohio, (2015).
63. P. A. Kobryn and S. Semiatin, *Solid Freeform Fabrication Symposium Proceedings* (2001), p. 179–186.
64. S. Shao, M.J. Mahtabi, N. Shamsaei, and S.M. Thompson, *Comput. Mater. Sci.* 131, 209 (2017).
65. H.V. Atkinson and S. Davies, *Metall. Mater. Trans. A* 31, 2981 (2000).
66. M. Dallago, V. Fontanari, B. Winiarski, F. Zanini, S. Carmignato, and M. Benedetti, *Procedia Struct. Integr.* 7, 116 (2017).
67. M. Kahlin, H. Ansell, and J.J. Moverare, *Int. J. Fatigue* 103, 353 (2017).
68. A. Bagheri, M.J. Mahtabi, and N. Shamsaei, *J. Mater. Process. Technol.* 252, 440 (2018).
69. E. Brandl, C. Leyens, and F. Palm, *IOP Conf. Ser. Mater. Sci. Eng.* 26, 1 (2011).
70. X. Wu, J. Liang, J. Mei, C. Mitchell, P.S. Goodwin, and W. Voice, *Mater. Des.* 25, 137 (2004).
71. C. Selcuk, *Powder Metall.* 54, 94 (2011).
72. L.M. Gammon, R.D. Briggs, J.M. Packard, K.W. Batson, R. Boyer, and C.W. Domby, *Metallography and Microstructures of Titanium and Its Alloys*, ASM Handbook, Vol. 9: *Metallography and Microstructures* (ASM International: Materials Park, 2004), p. 899.
73. I. Polmear, D. St. John, J.-F. Nie, and M. Qian, *Light Alloys: Metallurgy of the Light Metals* (London: Butterworth-Heinemann, 2017).
74. W. Xu, M. Brandt, S. Sun, J. Elambasseril, Q. Liu, K. Latham, K. Xia, and M. Qian, *Acta Mater.* 85, 74 (2015).
75. J. Gockel, and J. Beuth, *Solid Freeform Fabrication Symposium Proceedings* (2013), p. 666.
76. J. Gockel, J. Beuth, and K. Taminger, *Addit. Manuf.* 1–4, 119 (2014).
77. F. Wang, S. Williams, P. Colegrove, and A.A. Antonysamy, *Metall. Mater. Trans. A* 44, 968 (2013).
78. T. Wang, Y.Y. Zhu, S.Q. Zhang, H.B. Tang, and H.M. Wang, *J. Alloys Compd.* 632, 505 (2015).
79. U. Zerbst and K. Hilgenberg, *Procedia Struct. Integr.* 7, 141 (2017).
80. S. Beretta and S. Romano, *Int. J. Fatigue* 94, 178 (2017).
81. Y. Murakami, *Int. J. Fatigue* 41, 2 (2012).
82. B.M. Schöbauer, H. Mayer, K. Yanase, and M. Endo, *Procedia Struct. Integr.* 7, 492 (2017).
83. H. Kitagawa and S. Takahashi, in *Proceedings of International Conference on Mechanical Behaviour of Materials, 2nd* (1976), p. 627.
84. U. Zerbst, M. Madia, and H.T. Beier, *Eng. Fract. Mech.* 130, 6 (2014).
85. U. Zerbst, M. Vormwald, R. Pippan, H.P. Gänser, C. Sarrazin-Baudoux, and M. Madia, *Eng. Fract. Mech.* 53, 190 (2016).
86. K.J. Miller, *Fatigue Fract. Eng. Mater. Struct.* 5, 223 (1982).
87. K.J. Miller, *Mater. Sci. Technol.* 9, 453 (1993).
88. M.H. El Haddad, T.H. Topper, and K.N. Smith, *Eng. Fract. Mech.* 11, 573 (1979).
89. Y. Murakami, K. Takahashi, and T. Yamashita, *Trans. Jpn. Soc. Mech. Eng. A* 63, 1612 (1997).
90. D. Greitemeier, C. Donne Dalle, F. Syassen, J. Eufinger, and T. Melz, *Mater. Sci. Technol.* 32, 629 (2016).
91. R.G. Forman and S.R. Mett, NASA TM 102165, National Aeronautics and Space Administration (1990).
92. H. Neuber, *Theory of Notch Stresses* (Berlin: Springer, 1957).
93. R.E. Peterson, Notch sensitivity. *Metal Fatigue*, ed. G. Sines and J.L. Waisman (New York: McGraw Hill, 1959), p. 293.
94. S.D. Sheppard, *Trans. ASME* 113, 188 (1991).
95. D. Taylor, *Int. J. Fatigue* 21, 413 (1999).
96. L. Susmel and D. Taylor, *Fatigue Fract. Eng. Mater. Struct.* 30, 567 (2007).

97. Y. Xue, C.L. Burton, M.F. Horstemeyer, D.L. McDowell, and J.T. Berry, *Metall. Mater. Trans. B* 38, 601 (2007).
98. M. Lugo, J.E. Fountain, J.M. Hughes, J.-L. Bouvard, and M.F. Horstemeyer, *J. Appl. Polym. Sci.* 131, 1 (2014).
99. J. Simsiriwong, R. Shrestha, N. Shamsaei, M. Lugo, and R.D. Moser, *J. Mech. Behav. Biomed. Mater.* 51, 388 (2015).
100. M.A. Bagheri, Ph.D. Dissertation, Mississippi State University (2017).
101. H. Mughrabi, *Procedia Eng.* 2, 3 (2010).
102. C. Laird, P. Charsley, and H. Mughrabi, *Mater. Sci. Eng.* 81, 433 (1986).
103. H. Mughrabi, *Acta Metall.* 31, 1367 (1983).
104. D. Kuhlmann-Wilsdorf, *Mater. Sci. Eng. A* 113, 1 (1989).
105. M.A. Meyers and K.K. Chawla, *Mechanical Behavior of Materials*, 2nd ed. (Cambridge: Cambridge University Press, 2007).
106. M.W. Tofique, J. Bergström, and C. Berman, *Procedia Struct. Integr.* 2, 1181 (2016).
107. V. Kazymyrovych, J. Bergström, and C. Burman, *Steel Res. Int.* 81, 308 (2010).
108. S.K. Ås, B. Skallerud, and B.W. Rveiten, *Int. J. Fatigue* 30, 2200 (2008).
109. H. Neuber, *Theory of Notch Stresses: Principles for Exact Calculation of Strength with Reference to Structural Form and Material*, 2nd ed. (Berlin: Springer, 1958).
110. R.E. Peterson, *Exp. Mech.* 1, 105 (1961).
111. R.E. Peterson, *Stress Concentration Factors* (New York: Wiley, 1974).
112. S.K. Ås, B. Skallerud, B.W. Tveiten, and B. Holme, *Int. J. Fatigue* 27, 1590 (2005).
113. J.E. Siebel and M. Stieler, *VDI-Z* 97, 121 (1955).
114. B. Zhang, K. Ham, S. Shao, N. Shamsaei, and S. M. Thompson, *Solid Freeform Fabrication Symposium Proceedings* (2017), p. 107.
115. Y. Tian, D. McAllister, H. Colijin, M. Mills, D. Farson, M. Nordin, and S. Babu, *Metall. Mater. Trans. A* 45, 4470 (2014).
116. W.J. Sames, K.A. Unocic, R.R. Dehoff, T. Lolla, and S.S. Babu, *J. Mater. Res.* 29, 1920 (2014).
117. A.M. Hussein and J. El-Awady, *Int. J. Fatigue* 87, 339 (2016).
118. J. El-Awady, N.M. Ghoniem, and H. Mughrabi, *Materials Processing and Manufacturing Division Symposium* (2007), p. 23.
119. A.M. Hussein and J. El-Awady, *J. Mech. Phys. Solids* 91, 126 (2016).
120. C. Déprés, C.F. Robertson, and M.C. Fivel, *Mater. Sci. Eng. A* 387, 288 (2004).
121. M. Verdier, M.C. Fivel, and I. Groma, *Model. Simul. Mater. Sci. Eng.* 6, 755 (1998).
122. C.F. Robertson, M.C. Fivel, and A. Fissolo, *Mater. Sci. Eng. A* 315, 47 (2001).
123. C. Déprés, C.F. Robertson, and M.C. Fivel, *Philos. Mag.* 86, 79 (2006).
124. C. Déprés, C.F. Robertson, and M.C. Fivel, *Philos. Mag.* 84, 2257 (2004).
125. C. Déprés, C.F. Robertson, and M.C. Fivel, *Aerosp. Lab* 9, 1 (2015).
126. S. Shao, A. Misra, H. Huang, and J. Wang, *J. Mater. Sci.* 53, 5546 (2018).
127. J. Wang, H. Huang, and T.S. Cale, *Model. Simul. Mater. Sci. Eng.* 12, 1209 (2004).
128. M. Rhee, H.M. Zhib, J.P. Hirth, H. Huang, and T. de la Rubia, *Model. Simul. Mater. Sci. Eng.* 6, 467 (1998).
129. G.M. Castelluccio, W.D. Musinski, and D.L. McDowell, *Curr. Opin. Solid State Mater. Sci.* 18, 180 (2014).
130. G.M. Castelluccio and D.L. McDowell, *Mater. Sci. Eng. A* 598, 34 (2014).